の直流電流により細胞膜にナノサイズの小孔をあけて細胞をアポトーシスに至らせるため，RFAなどの熱ablation治療のように，血管・胆管といった周辺重要臓器の線維性の構築を破壊しない．そのため，治療域に血流が残存し，ablationされた領域の評価が困難となる．実際に本症例でも，治療域と思われる領域の内部に血流が残存しており，CT，MRI，造影超音波の血管相では，治療域の評価は困難であった．一方ソナゾイド造影超音波のKupffer相や，EOB-MRIの肝細胞相で治療域が明瞭に描出され，治療域の評価に有用であった(Fig. 1)．しかし，今後IRE治療症例を集積し検討していく必要がある．

索引用語：肝細胞癌，不可逆電気穿孔法，造影超音波

文献：1）Lee EW, Chen C, Prieto VE, et al. Radiology 2010; 255: 426—433　2）Rubinsky B, Onik G, Mikus P. Technol Cancer Res Treat 2007; 6: 37—48　3）Cannon R, Ellis S, Hayes D, et al. J Surg Oncol 2013; 107: 544—554

本論文内容に関連する著者の利益相反：なし

英文要旨

A case of hepatocellular carcinoma successfully treated by irreversible electroporation

Katsutoshi Sugimoto[1]*, Fuminori Moriyasu[1], Mayumi Ando[1], Takatomo Sano[1], Yuki Miyata[1], Junichi Taira[1], Yoshiyuki Kobayashi[2], Yasuharu Imai[1], Ikuo Nakamura[1]

We report a woman in her late 60s with hepatocellular carcinoma in whom the tumor was successfully treated by irreversible electroporation (IRE). Vascular-phase contrast-enhanced US (CEUS) with Sonazoid and dynamic CT at 1 day after treatment showed no tumor enhancement, but the safety margin of ablation appeared to be insufficient. On the other hand, in Kupffer-phase CEUS, the ablation zone showed a clear contrast defect with a sufficient ablation margin, indicating cell death of hepatocytes, cancer cells, and Kupffer cells in this area following IRE treatment. Very similar findings were observed in hepatobiliary-phase Gd-EOB-DTPA-enhanced MRI at 7 days after treatment. These results suggest that both Kupffer-phase CEUS and hepatobiliary-phase Gd-EOB-DTPA-enhanced MRI may be useful for assessing the ablation zone in patients who have undergone IRE.

Key words: hepatocellular carcinoma, IRE, contrast-enhanced ultrasound

Kanzo 2014; 55: 290—292

1）Department of Gastroenterology and Hepatology, Tokyo Medical University, Tokyo, Japan
2）Department of Gastroenterology and Hepatology, Tokyo Medical University Hachioji Medical Center, Tokyo, Japan
*Corresponding author: sugimoto@tokyo-med.ac.jp

〔第二世代画像強調内視鏡の臨床的意義〕

第二世代NBI：有用性と使用方法のコツ
—細径経鼻内視鏡観察—

河合　隆*　佐藤丈征*,**　八木健二**　福澤誠克*,**
草野　央**　後藤田卓志　森安史典

要旨　いわゆる第二世代とされる細径経鼻内視鏡であるGIF-XP290N(＋EVIS LUCERA ELITE system)は第一世代経鼻内視鏡であるXP260N(＋EVIS LUCERA SPECTRUM system)と比較すると，超近接観察(至近距離3 mm)にて，明らかな解像度の差を認めた。さらに，NBI併用超近接観察では，咽頭・食道病変の扁平上皮病変においては，これまでは腫瘍病変部をbrownish area(BA)としてのみ視認可能であったが，XP290NではBAの視認ばかりでなく，日本食道学会の新分類のType Bに相当する血管変化を視認することが可能である。また，Barrett食道・胃病変の腺上皮病変においては，これまで不可能であった粘膜構造変化を捉えることが可能である。スクリーニング内視鏡である経鼻内視鏡に新しい診断技術が追加された。

key words：経鼻内視鏡，NBI，Barrett食道，胃癌

緒　言

近年，上部消化管のスクリーニングにおいて，苦痛が少なく，循環動態に及ぼす影響も少ない[1]ことから，経鼻内視鏡検査が広く使用されている。しかし，細径であるがために解像度を中心として，画像が経口内視鏡に比べ劣ることが問題とされてきた。

近年開発された，新しい細径経鼻内視鏡であるGIF-XP290N＋Olympus LUCERA ELITE systemが，この点においてどの程度改善がみられるかを検討した。

Ⅰ．Olympus LUCERA ELITE systemおよびXP290N

LUCERA ELITE systemでは，明るさが格段に上がった。特にNBIを使用する場合，以前のXP260N(＋EVIS LUCERA SPECTRUM system)では，暗くてとても遠景観察診断に用いることができなかったが，キセノンランプの改善，NBI観察光の照射方法として，二重露光の採用，光学設計の改善により，NBIの明るさも向上している。実際に，明るさが不十分であった遠点の被写体も，より明るく観察することが可能になっている(**図1**)。

細径経鼻内視鏡においても，GIF-XP290N＋Olympus LUCERA ELITE systemの併用により，光源光量が明るくなったことから，近接時にコントラストが低下しない対物光学系を採用している。したがって，従来細径スコープと比較して超近接時(3 mm)はGIF-H260並みの解像力を実現することが可能となっている[2](**図2**)。

さらに，XP290Nにおいて，超近接観察時にNBI併用観察をすることが大きなポイントである。方法としては，通常の白色光観察にて病変を認めた場合(**図3**a)，NBI観察に切り替える(図3b)。その後，細

* 東京医科大学病院内視鏡センター　** 同 消化器内科
〔〒160-0023 東京都新宿区西新宿6-7-1〕

a|b

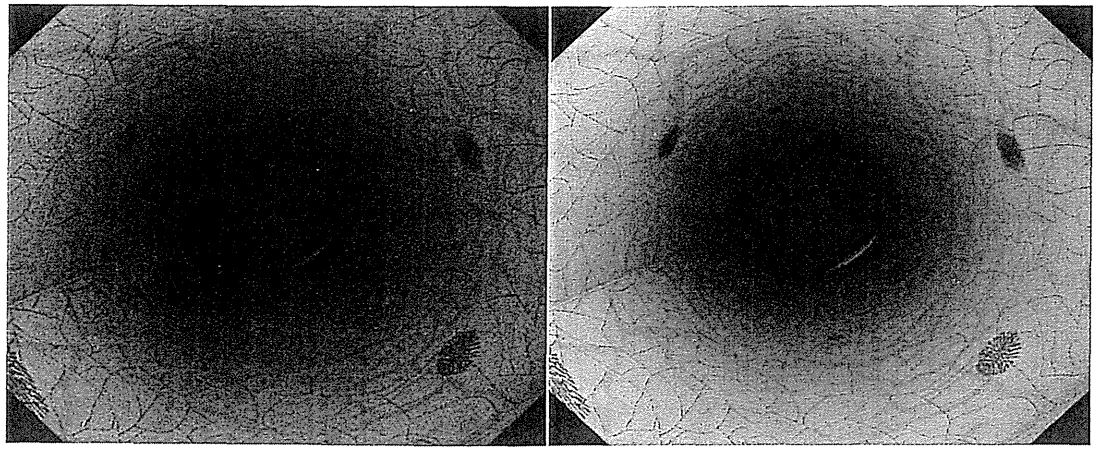

図1　システムによるNBI強調画像の比較
a. EVIS LUCERA SPECTRUM　b. EVIS LUCERA ELITE
（オリンパスメディカルシステムズ社資料）

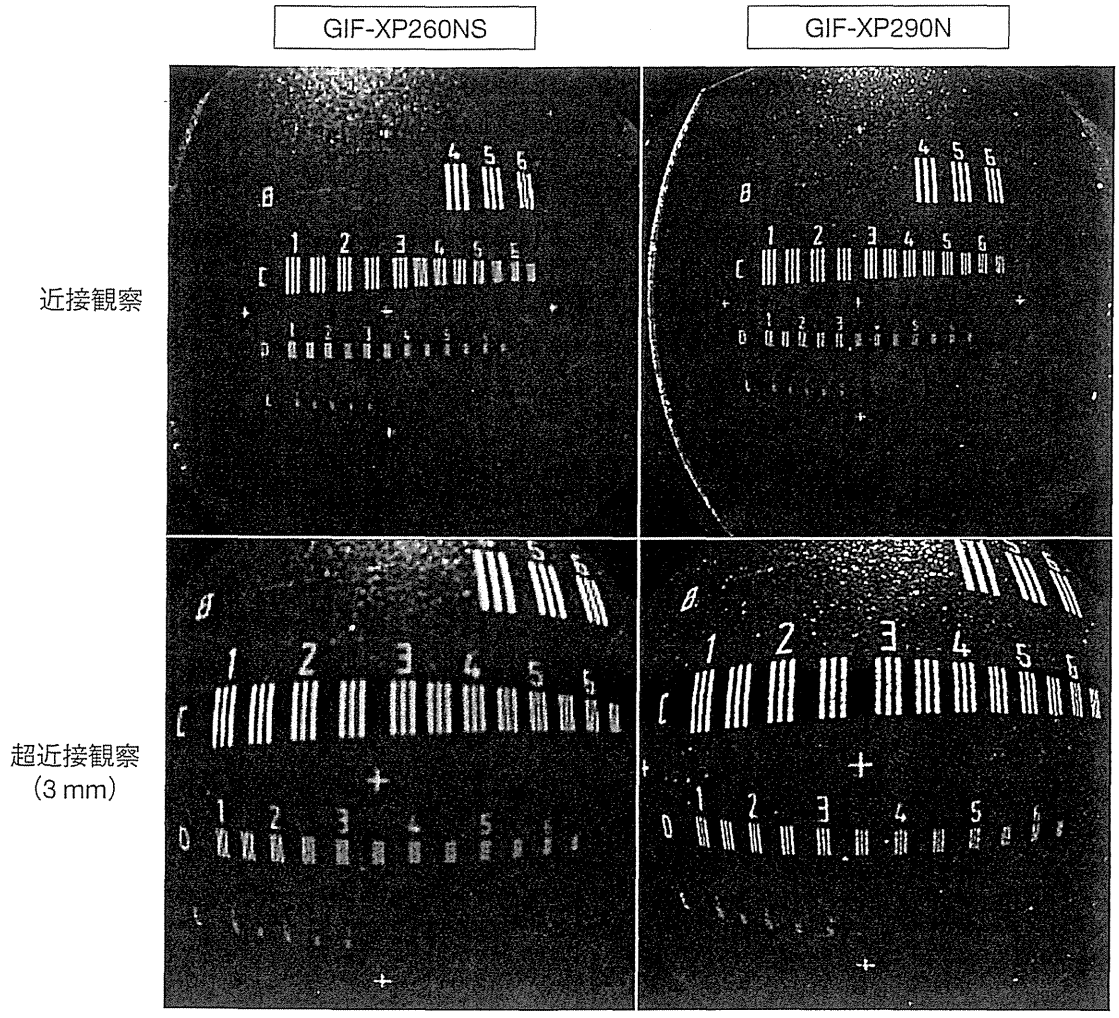

図2　従来細径スコープ(XP260NS)とXP290Nの解像度の比較

径スコープをゆっくり病変部分に近づけて観察距離　　る(図3c)。
を3 mmにすると，詳細な粘膜構造の画像が得られ

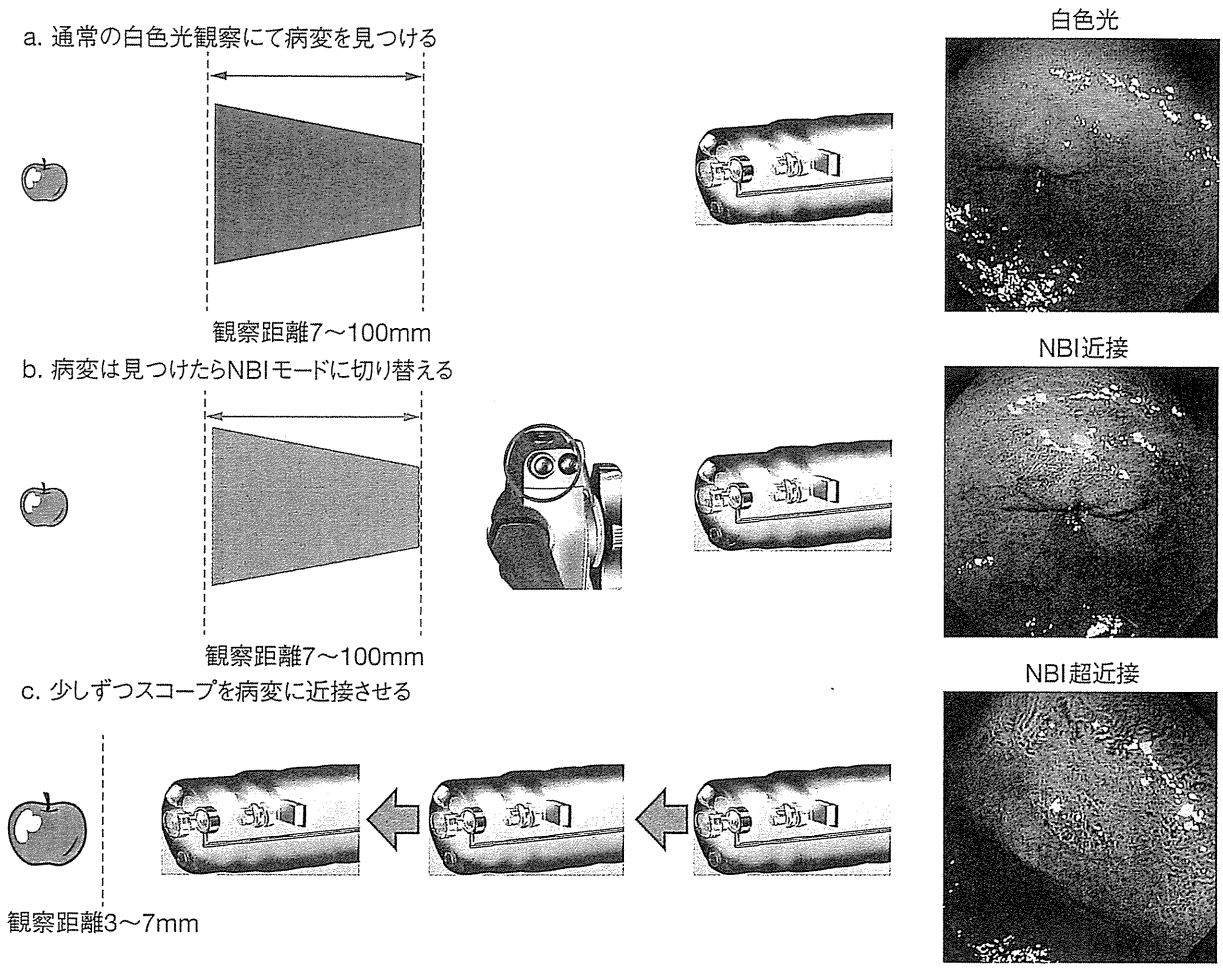

図3　GIF-XP290Nの使い方(超近接観察)

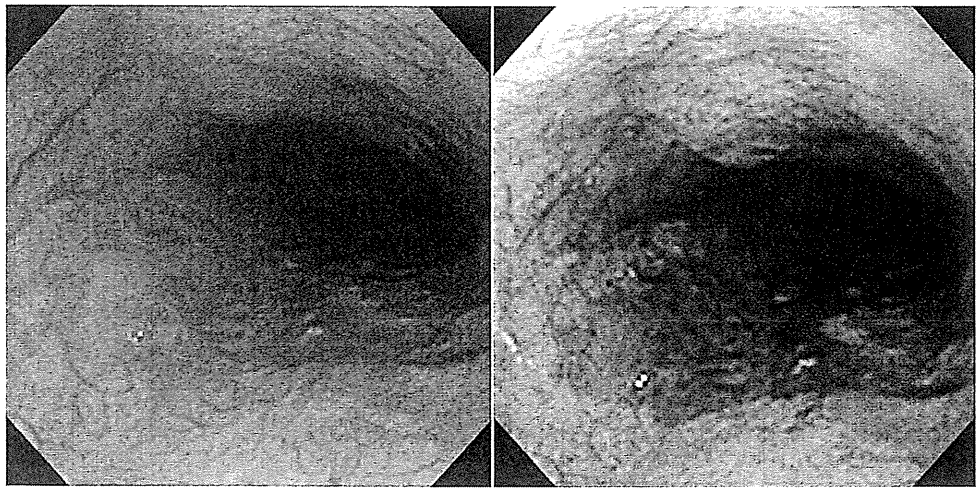

a|b

図4　早期食道癌
(GIF-XP260NS使用)
a．白色光観察像
b．NBI観察像

Ⅱ．扁平上皮病変(食道・咽頭)

図4に70歳代の男性，早期食道癌症例の内視鏡写真を示す。白色光観察(図4a)では4～10時方向にかけて，淡い発赤と血管透見像の消失を認める。一方，図4bのNBI併用観察では，同部位がbrownish area

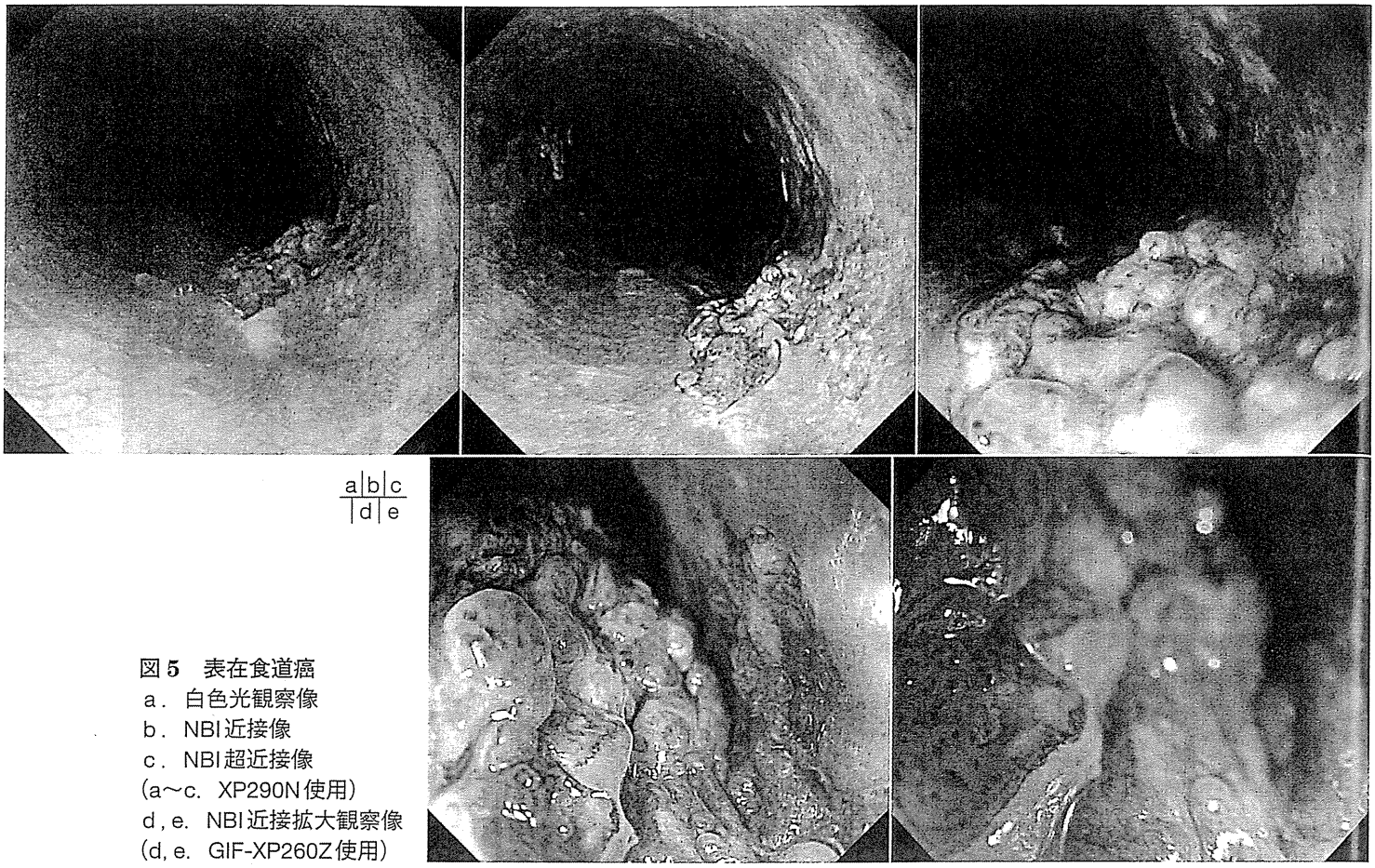

図5 表在食道癌
a．白色光観察像
b．NBI近接像
c．NBI超近接像
(a～c．XP290N使用)
d, e．NBI近接拡大観察像
(d, e．GIF-XP260Z使用)

(BA)となり，病変の視認性が明らかに向上している。筆者らはこのようにXP260N(＋EVIS LUCERA SPECTRUM system)においても，NBI観察を併用することにより，有意に食道病変を発見できることを報告した。しかし，従来の経鼻内視鏡NBI併用観察では，食道病変の視認が可能であるが，病変部にこれ以上近づくことができず(ピントが合わない)，したがって癌の確定診断は不可能であった。

一方，XP290Nでは，先に述べたようにNBIを併用し，超近接観察すると，扁平上皮病変においては，日本食道学会の新分類[3]のType B(血管形態の変化が高度なもの)に相当する血管変化を視認することが可能である。

症例は60歳代の男性，表在食道癌である(**図5**)。図5aに示すように，白色光観察においても不整な凹凸の病変を認めた。NBIを併用し超近接観察すると，凹凸粘膜内にType B1あるいはType B2と思われる異常血管を認めることが可能であり(図5b，c)，扁平上皮癌と診断できる。図5d，eは同症例の拡大内視鏡を示すが，XP290Nの内視鏡写真と同様な異常血管を認めた。

図6は40歳代の女性の中咽頭癌の内視鏡写真である。白色光観察にて中咽頭後壁に発赤粘膜を認める(図6a)。NBIに切り替えると同部位にType Bに相当する異常血管を認めた(図6b)。さらに超近接観察により，ドット状の異常血管が容易に観察可能であり(図6c矢印)，扁平上皮癌と診断できる。

Ⅲ．腺上皮病変(Barrett食道・胃)

1．Barrett食道粘膜の観察

従来の経鼻内視鏡であるXP260Nシリーズにおいても Barrett食道(BE)を診断することは可能である。

胃潰瘍の経過観察のために，定期的に内視鏡検査を受ける60歳代の男性の症例を呈示する。GIF-XP260NS＋EVIS LUCERA SPECTRUM(以下，260NS)systemで前回撮影した画像(**図7**a，b)(白色

a|b|c

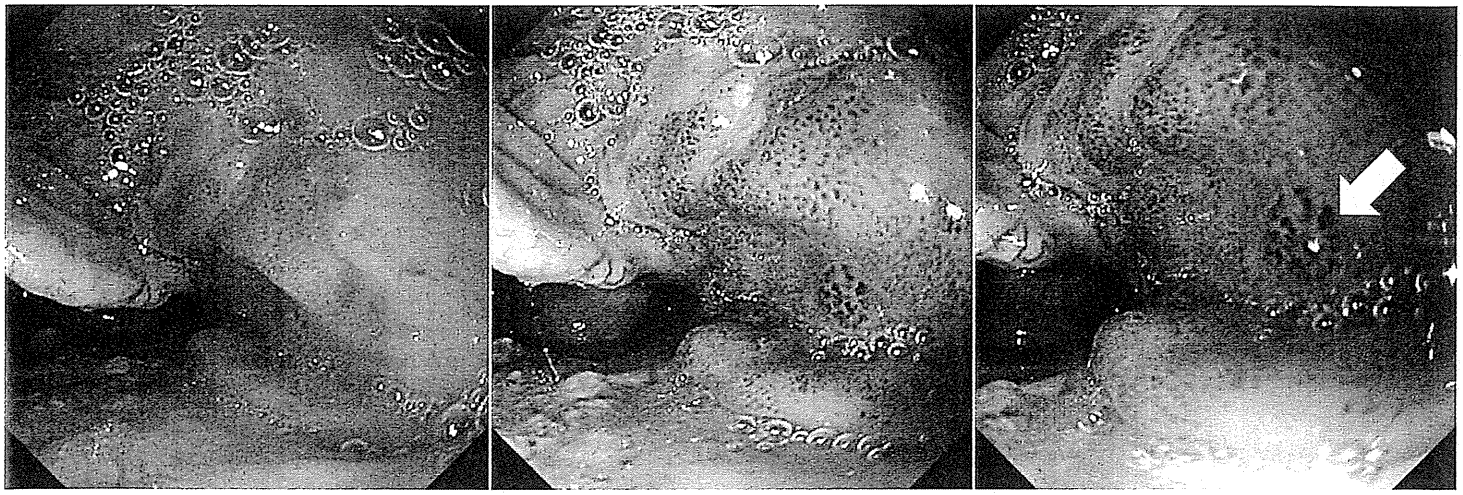

図 6　中咽頭癌(GIF-XP290N使用)
a. 白色光観察像　b. NBI近接像　c. NBI超近接像

a|b
c|d|e

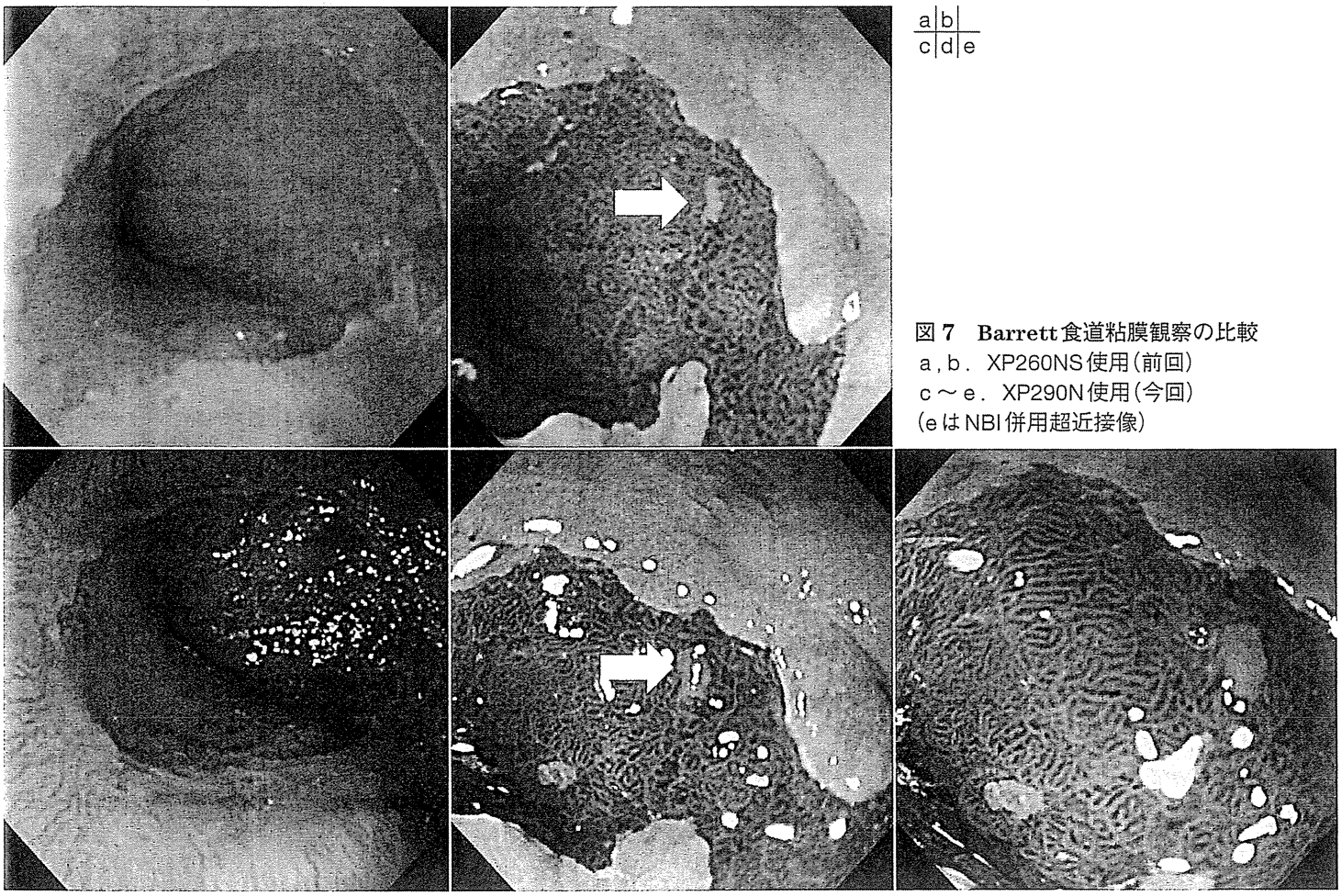

図 7　Barrett食道粘膜観察の比較
a, b. XP260NS使用(前回)
c～e. XP290N使用(今回)
(eはNBI併用超近接像)

光＋NBI近接観察)と，今回GIF-XP290N＋EVIS LUCERA ELITE systemにて撮影した画像(図7c, d)(白色光＋NBI近接観察)を比較検討した。両者において，BEは進展なく，ほぼ同様な状態であるが，図7bのNBI近接観察(260NS)では，扁平上皮島の存在診断はかろうじて可能であるが，粘膜の構造は把

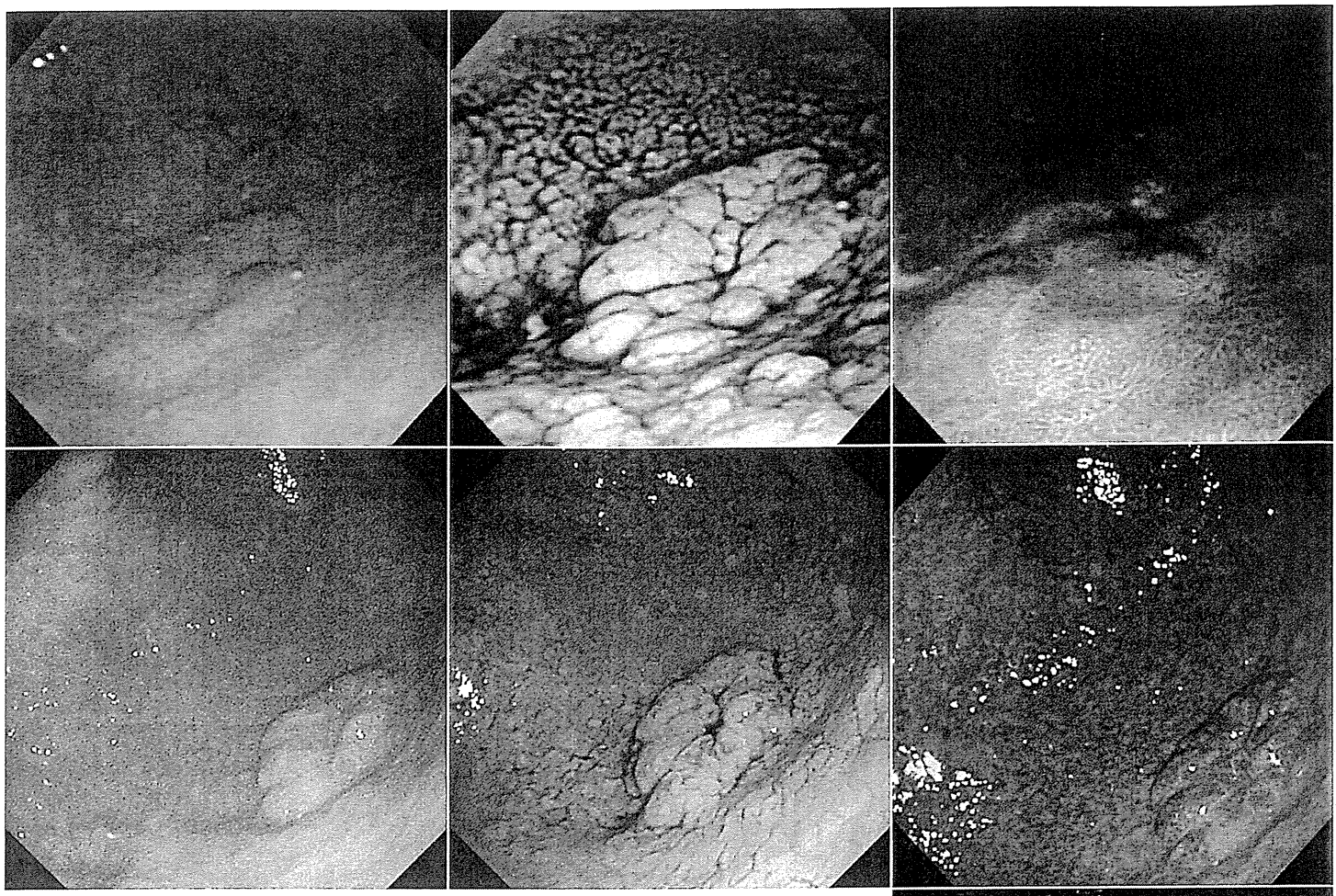

図8　胃腺腫内癌(tub1, pT1a(M), ly0, v0, pHM0, pVM0)
a～c. XP260NS使用　d～g. XP290N使用
a, d. 白色光観察像　b, e. インジゴカルミン色素像　c, f～h. NBI観察像
(g. NBI近接像　h. 超近接像)

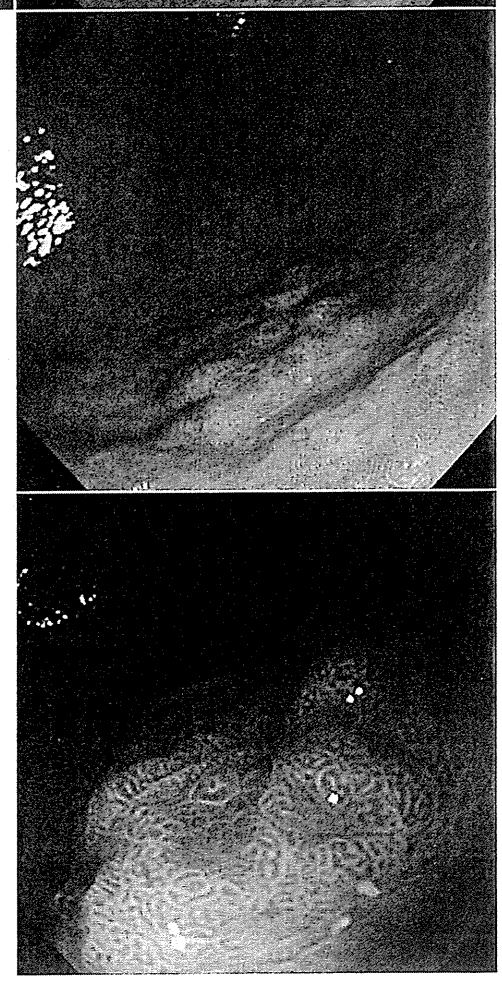

a b c
d e f
g
h

握できない。

一方, 290Nでは, 容易に扁平上皮島の診断は可能である。さらに3 mmにNBI併用超近接観察をした場合, 290Nでは扁平上皮島の存在も明瞭になるとともに, 粘膜構造をも観察可能である(図7e)。

2．胃腫瘍性病変

症例は80歳代男性。腺腫内癌の症例である。XP260NS(**図8**a～c)とXP290N(図8d～f)の画像を比較したものだが, 一目見ただけで, XP290Nは, 白色光においてもXP260NSに比べて明るく, 病変もきれいに見える(図8a, d)。ただし, インジゴカルミン色素散布では, XP260NSとXP290Nの画像に明らかな差は認めない(図8b, e)。NBIも通常の近接観察では, XP260NSに比べ多少きれいに見えるだけである(図8c, f)。しかし, XP290Nでは, 超近接観察ができることで, これまでの経鼻胃内視鏡では不可能であった病変部の粘膜構造を観察することができた

(図8g, h)。この症例では一部の粘膜構造の不明瞭化を認めた[4]。

ま と め

新しい細径経鼻内視鏡であるXP290Nは，GIF-H260並みの解像力を実現することが可能であるが，その機能を発揮するためには，NBIを併用し，至近距離(3 mm)で観察することが必要である。

文 献

1. Kawai T, Miyazaki I, Yagi K et al: Comparison of the effects on cardiopulmonary function of ultrathin transnasal versus normal diameter transoral esophagogastroduodenoscopy in Japan. Hepatogastroenterology **54**: 770-774, 2007
2. Kawai T, Fukuzawa M, Gotoda T: Evolution of ultrathin endoscope. Dig Endosc **25**(4): 46, 2013
3. 日本食道学会(編): 食道癌 診断・治療のガイドライン. 金原出版，東京，2012
4. Kawai T, Yanagisawa K, Fukuzawa M et al: Evaluation of gastric cancer diagnosis using ultrathin transnasal endoscopy with narrow-band imaging. DDW2014, Sa1871

Usefulness and Technique of NBI Second Version: Ultrathin Transnasal Endoscopy

Takashi KAWAI*, Takemasa SATOU*,**, Kenji YAGI**, Masakatsu FUKUZAWA*,**, Chika KUSANO**, Takuji GOTODA, and Fuminori MORIYASU

**Endoscopy Center, **Department of Gastroenterology and Hepatology, Tokyo Medical University Hospital, Tokyo, Japan*

There are clearly difference of resolution on super close observation(3 mm)between GIF-XP290N(+EVIS LUCERA ELITE system)and XP-260N(+EVIS LUCERA SPECTRUM system). We can detect abnormal vessels-so-called "Type B"-based on the new classification system of the Japan Esophageal Society for squamous epithelial lesions in the pharyngo-esophageal area. We can also detect mucosal patterns for gastric gland epithelial lesions in Barrett's esophagus and the stomach. This is a new diagnostic technique for transnasal endoscopy.

kew words: transnasal endoscopy, NBI, Barrett's esophagus, gastric cancer

Legends to Figures

Figure 1 Comparison of image-enhancing endoscopy between EVIS LUCERA SPECTRUM and EVIS LUCERA ELITE.

Figure 2 Comparison of resolution between GIF-XP260NS and GIF-XP290N with reference to close observation.

Figure 3 Method of use for GIF-XP290N with reference to super close observation.
a. Detection of the lesion with white light.
b. Change to NBI mode after detection of the lesion.
c. Super-close observation of the lesion at a slow pace.

Figure 4 Comparison of endoscopic image between white light and NBI in early esophageal cancer using GIF-XP260NS.

Figure 5 a-c. Comparison of endoscopic image between white light, NBI close, and NBI super-close observation in superficial esophageal cancer using GIF-XP290N.
d, e. Endoscopic image of NBI magnification in superficial esophageal cancer using GIF-H260Z.

Figure 6 Comparison of endoscopic image between white light, NBI close and NBI super close in pharyngeal cancer using GIF-XP290N.

Figure 7 a-d. Comparison of endoscopic image between GIF-XP260NS and GIF-XP290N in Barrett's esophagus.
e. Comparison of endoscopic image between NBI close observation and NBI super close observation in Barrett's esophagus using GIF-XP290N.

Figure 8 a-f. Comparison of endoscopic image between white light, indigocarmine dye-staining and NBI close for cancer in adenoma using GIF-XP260NS and GIF-XP 290N.
g, h. Comparison of endoscopic image between NBI close observation and NBI super close observation for cancer in adenoma using GIF-XP290N.

ELSEVIER

CrossMark

Ultrasound in Med. & Biol., Vol. 40, No. 6, pp. 1089–1095, 2014

0301-5629/$ - see front matter

http://dx.doi.org/10.1016/j.ultrasmedbio.2013.12.019

● *Original Contribution*

KUPFFER-PHASE FINDINGS OF HEPATIC HEMANGIOMAS IN CONTRAST-ENHANCED ULTRASOUND WITH SONAZOID

KATSUTOSHI SUGIMOTO,* FUMINORI MORIYASU,* KAZUHIRO SAITO,† HIROKI YOSHIARA,‡ and YASUHARU IMAI*

*Department of Gastroenterology and Hepatology, Tokyo Medical University, Tokyo, Japan; †Department of Radiology, Tokyo Medical University, Tokyo, Japan; and ‡Ultrasound Division, Toshiba Medical Systems Corporation, Tochigi, Japan

(*Received* 23 *May* 2013; *revised* 12 *November* 2013; *in final form* 12 *December* 2013)

Abstract—The aim of this study was to assess quantitatively the Kupffer-phase enhancement patterns of hepatic hemangiomas in contrast-enhanced ultrasound (CEUS) with Sonazoid. A total of 46 patients with 46 hepatic hemangiomas (17.1 ± 6.2 mm in diameter, 34 typical type and 12 high-flow type) underwent CEUS in the Kupffer phase. The lesion-to-liver contrast ratio in the Kupffer phase was quantitatively assessed for both types of hemangioma. Most of the hepatic hemangiomas, whether or not they were the high-flow type, were iso- to hypo-echoic relative to the surrounding liver parenchyma. The contrast ratio was −5.33 ± 6.70 dB for the high-flow hemangiomas and −4.54 ± 6.28 dB for the typical hemangiomas. There was no significant difference in contrast ratio between the two types of lesions (p = 0.73). All of the hemangiomas, whether of typical or high-flow type, are iso- to hypo-echoic relative to the surrounding liver parenchyma on Kupffer-phase imaging.
(E-mail: sugimoto@tokyo-med.ac.jp)

Key Words: **Hemangioma, Liver, Ultrasound, Contrast, Sonazoid, High-flow type, Kupffer phase.**

INTRODUCTION

Contrast-enhanced ultrasound (CEUS) has markedly improved the diagnosis of hemangiomas because enhancement patterns during the arterial, portal venous and late phases can be observed, permitting the correct diagnosis to be obtained in about 95% of cases (Strobel et al. 2008). The typical CEUS feature of hemangiomas is peripheral nodular enhancement in the arterial phase, progressing in the centripetal direction to partial or complete fill-in. The fill-in enhancement lasts from seconds to minutes and is more rapid in smaller lesions. Enhancement is sustained through the late phases.

On the other hand, high-flow hemangiomas, which account for 16% of all hemangiomas and 42% of hemangiomas less than 1 cm in diameter, exhibit rapid homogeneous hyper-enhancement in the arterial phase and can be confused with focal nodular hyperplasia (FNH) or, rarely, with hepatocellular adenomas (HCAs) or carcinomas (Dietrich et al. 2007).

The contrast agents currently used in diagnostic US examinations of the liver are microbubbles consisting of gas bubbles stabilized by a shell, such as SonoVue (Bracco, Milan, Italy), Definity (Lantheus Medical, Billerica, MA, USA) and Sonazoid (Daiichi-Sankyo, GE, Tokyo, Japan). These contrast agents exhibit similar behavior in CEUS imaging, with rapid enhancement of the vascular pool after intravenous injection and slow dissipation over about 5 min (Cosgrove and Harvey 2009).

An exception to this typical behavior occurs with Sonazoid. It has an extended late phase (hereinafter termed the *post-vascular phase*) in which it persists for several hours in the liver, long after it has become undetectable in the vascular pool. Sonazoid can be phagocytosed by Kupffer cells, and this undoubtedly contributes to its persistence in the liver. The post-vascular phase is therefore also referred to as the *Kupffer phase* (Yanagisawa et al. 2007).

To the best of our knowledge, there have been no reports concerning the enhancement patterns of hemangiomas in the Kupffer phase, even though there have been many investigations on their enhancement patterns in

Address correspondence to: Katsutoshi Sugimoto, Department of Gastroenterology and Hepatology, Tokyo Medical University, 6-7-1 Nishishinjuku, Shinjuku-ku, Tokyo 160-0023, Japan. E-mail: sugimoto@tokyo-med.ac.jp

Conflicts of Interest: The authors have indicated that they have no conflicts of interest regarding the content of this article.

the vascular phases (*i.e.,* arterial, portal venous and late phases) (Dietrich et al. 2007; Moriyasu and Itoh 2009; Strobel et al. 2008).

Therefore, the aims of the present study were as follows: first, to assess quantitatively the Kupffer-phase enhancement patterns of hepatic hemangiomas in CEUS with Sonazoid, and second, to assess quantitatively the differences in enhancement patterns between high-flow and typical hemangiomas in the Kupffer phase.

METHODS

Patients

This retrospective study was approved by our institutional review board, and informed consent from the patients was waived. One author (H.Y.) is a researcher at Toshiba who provided technical support and advice concerning image analysis.

We identified 1448 consecutive patients who underwent CEUS with Sonazoid of the liver at our institution from January 2007 to August 2010. All patients had been referred for CEUS to evaluate suspected liver disease. The selection criteria for inclusion in this study were as follows: first, reliable evidence of a hepatic hemangioma was confirmed based on the diagnostic criteria described below; second, the maximum diameter of the lesion was 3 cm or less; third, only one tumor per patient was studied, with the tumor selected on the basis of its size and site (providing the best acoustic window for image acquisition); and fourth, all patients had normal liver function, with no underlying chronic liver disease, including fatty liver.

The diagnosis of hemangioma was established based on a combination of imaging findings: a classic contrast enhancement pattern observed on dynamic computed tomography and/or CEUS, with peripheral nodular enhancement or tiny enhancing dots in the early phase and persistent enhancement or centripetal fill-in enhancement in the delayed phase (Kim et al. 2001; Strobel et al. 2008), or uniform early enhancement observed on dynamic computed tomography and/or CEUS, hyperintensity relative to liver parenchyma in heavily T2-weighted magnetic resonance imaging (Sasaki et al. 2005), and follow-up image findings showing stability for at least 6 mo. These two sets of criteria were used to establish the presence of typical hepatic hemangiomas and high-flow hepatic hemangiomas, respectively.

A total of 46 hepatic hemangiomas in 46 patients were evaluated in this study. The lesions measured 19.7 ± 6.2 mm (mean ± SD) in diameter. Of the hepatic hemangiomas studied, 34 were the typical type (mean diameter = 20.8 mm), with peripheral nodular enhancement progressing centripetally, and 12 were the high-flow type (mean diameter = 16.7 mm), with uniform enhancement in the arterial phase.

US imaging technique

All US scans were obtained by three sonologists (K. Sugimoto, Y.I. and F.M.) with 10, 11 and 15 y of experience, respectively, in standard US and CEUS. The US equipment used was an SSA-790 A (Aplio XG, Toshiba Medical Systems, Tochigi, Japan) with a 3.75-MHz convex transducer (PVT-375 BT, Toshiba). The imaging mode was wideband harmonic imaging (commercially called pulse subtraction) with transmission and reception frequencies of 1.75 and 3.5 MHz, respectively.

First, each lesion was scanned using B-mode US. The microbubble contrast agent Sonazoid was injected as a 0.5-mL bolus into an antecubital vein *via* a 21-gauge peripheral intravenous cannula, followed by a 10-mL saline flush. When a suspected lesion was identified, dynamic scanning was performed with the focus point set at the deeper end of the lesion at the rate of 15 frames/s and with a dynamic range of 45 dB. The mechanical index was between 0.2 and 0.3 to preserve the microbubbles throughout their half-life in the microvessels and to permit real-time assessment of the liver vasculature and parenchymal enhancement.

The lesion was observed continuously for about 3 min from the time of contrast injection (observation in the vascular phase), during which time we did not perform replenishment (*i.e.,* high-mechanical-index burst scan mode) to preserve the microbubbles. After 3 min, the scan was frozen. Then, after a waiting period of approximately 10 min from the injection of contrast agent to allow pooling of the agent in the liver parenchyma, the lesion was observed to evaluate enhancement using a sweep scan (observation in the Kupffer phase).

If a lesion could not be identified in the Kupffer phase because it was iso-echoic relative to the liver parenchyma, dual mode (which permits simultaneous display of a conventional B-mode image on one screen and contrast mode on the other) was used. The real-time images obtained in this study were stored on the hard disk of the US system. The images were also recalled from the cine loop memory and stored on a magneto-optical disk. Two sonologists (K. Sugimoto and Y.I.) each selected one cine loop per patient recorded in B-mode and Kupffer-phase images for off-site analysis.

Image analysis

The acquired time sequences of B-mode and contrast images were saved in Audio Video Interleaved (AVI) format. In the qualitative analysis, each lesion's B-mode appearance was subjectively assessed based on consensus between two sonologists (K. Sugimoto and Y.I.). The B-mode appearance was classified as follows: